Atmospheric Environment 167 (2017) 511–522

Contents lists available at ScienceDirect

Atmospheric Environment

journal homepage: www.elsevier.com/locate/atmosenv

Simulation and evaluation of dust emissions with WRF-Chem (v3.7.1) and its relationship to the changing climate over East Asia from 1980 to 2015

Hongquan Song [a, b, *], Kai Wang [b], Yang Zhang [b, **], Chaopeng Hong [b, c], Shenghui Zhou [a]

[a] Key Laboratory of Geospatial Technology for the Middle and Lower Yellow River Regions, Ministry of Education, Henan Key Laboratory of Integrated Air Pollution Control and Ecological Security, College of Environment and Planning, Henan University, Kaifeng, Henan 475004, China
[b] Department of Marine, Earth and Atmospheric Science, North Carolina State University, Raleigh, NC 27695, USA
[c] State Key Joint Laboratory of Environment Simulation and Pollution Control, School of Environment, Tsinghua University, Beijing 100084, China

HIGHLIGHTS

- A comprehensive evaluation of long-term simulations of dust emissions using surface data.
- Spatial-temporal variations of dust emissions in East Asia over the past four decades were simulated.
- Correlations between dust emissions and changing climate over East Asia were analyzed.

ARTICLE INFO

Article history:
Received 22 January 2017
Received in revised form
16 July 2017
Accepted 21 August 2017
Available online 24 August 2017

Keywords:
Wind erosion
Dust emission
Spatial-temporal variations
East Asia
Climate change

ABSTRACT

Dust particles have been long recognized to affect the atmospheric radiative balance and are influenced by climate change. Impacts of climate change on dust emissions in East Asia, however, are not well understood. In this work, we conduct an evaluation of meteorological variables and dust emissions using the Weather Research and Forecasting model coupled with chemistry (WRF-Chem) and examine the relationships between dust emissions and meteorological variables (wind speed, precipitation, and temperature) over East Asia during the period of 1980–2015. Model simulated surface meteorological variables compared well overall with surface-based observations, consistent with other WRF studies. Compared to observations, the coarse particulate matter ($PM_{10\text{-}2.5}$) concentrations were underpredicted for most dust source regions of East Asia with a domain-wide mean bias and correlation of $-40.2\ \mu g\ m^{-3}$ and 0.5 against observations, respectively. Dust particulate concentrations simulated by WRF-Chem were found to reproduce the observed spatial variability in surface dust particulates over East Asia. The average annual dust emission ($0 < r < 20\ \mu m$) is around 67.4 Tg yr^{-1} and the dust emission increased with the trend of 0.173 Tg yr^{-1} ($R^2 = 0.03$, $P = 0.32$) in China and Mongolia over the past four decades. The spatial and temporal variations of dust emissions in China and Mongolia indicate that the annual dust flux has increased in desert areas of China and Mongolia, but decreased in most Gobi regions of China. Dust emission is significantly positively and negatively correlated with wind velocity and precipitation at the regional scale. Spatial patterns of seasonal correlations between dust flux and climate varies greatly during the period of 1980–2015.

1. Introduction

Aeolian dust can modify the Earth's climate by altering the global energy budget (Lambert et al., 2013; Allen et al., 2016), influence global biogeochemical processes via nutrients transport (Wang et al., 2015), and affect air quality and human health (Lelieveld et al., 2015). Mineral dust in the atmosphere influences the radiative balance by directly scattering and absorbing incoming

* Corresponding author. College of Environment and Planning, Henan University, Jinming Campus, Kaifeng, Henan Province 475004, China.
** Corresponding author. #1125 Jordan Hall, Faucette Drive, Raleigh, NC 27695-8208, USA.
E-mail addresses: hqsong@henu.edu.cn (H. Song), yzhang9@ncsu.edu (Y. Zhang).

http://dx.doi.org/10.1016/j.atmosenv.2017.08.051
1352-2310/

solar radiation (Haywood et al., 2005) or indirectly changing the optical properties of clouds (Fiedler et al., 2015). Changing radiative balance can in turn alter regional winds and precipitation (Evan et al., 2014) and thus dust emissions, transport, and deposition processes (Zender and Kwon, 2005; Evan et al., 2016).

Dust storm is a type of severe natural disaster that frequently occurs in East Asia. During East Asian dust storm, large amounts of dust particles are emitted from arid and semiarid regions such as the Taklimakan Desert in northwestern China and the Gobi Desert in southern Mongolia (Yang et al., 2007), and frequently transported over long distances to the North Pacific Ocean, Korea, Japan, and as far as to the United States (Lee and Sohn, 2011; Pointing and Belnap, 2014; Nagashima et al., 2016). The amount of dust emitted from East Asia is approximately 20% of the global dust emissions (Nagashima et al., 2016). Dust storms occur most frequently during springtime in East Asia when surface conditions are dry and winds are strong (Sun et al., 2001; Kurosaki and Mikami, 2005). Understanding the linkages between dust and climate in the past will be crucial to predict dust emissions in East Asia under future climate conditions.

Dust emissions are generally controlled by the threshold friction velocity that is influenced by the combination of regional atmospheric and surface conditions, such as atmospheric stability, winds, precipitation, soil composition, soil moisture, and vegetation (Natsagdorj et al., 2003; Ravi et al., 2004; Ishizuka et al., 2005; Kok, 2011; Cowie et al., 2013; Kim and Choi, 2015). Numerous studies have been conducted to explore linkages between dust activities and climate (Lambert et al., 2008; Hoffman et al., 2014; Kim and Choi, 2015). Spatial and temporal patterns of dust storm frequency were generated from observed visibility and their linkages to climate changes based on meteorological observations have been investigated over the past several decades in China (Qian et al., 2002; Liu et al., 2004; Lim and Chun 2006; Yang et al., 2007; Lee and Sohn, 2011; Lee and Kim, 2012). Dust storm frequency used in past studies is a semi-quantitative indicator of dust emissions because it cannot continuously capture the strength of dust emissions during the whole study period and has limitations of observed accuracy. The surface measurements of visibility are not purely indicative of the dust particles nor are they always spatially and temporally homogeneous (Mahowald et al., 2007). However, the sensitivity of dust emissions to climate change and the underlying mechanisms in East Asia remain unclear over the past several decades.

This study simulates and extensively evaluates meteorological variables and particulate matter concentrations, and then analyzes the spatial patterns and temporal trends of the simulated vertical dust emission fluxes and meteorological variables (e.g., temperature, wind velocity, and precipitation) in China and Mongolia during the period of 1980–2015. The impacts of the changing climate variability on dust emissions are also examined through analyzing the relationships of simulated temperature, wind velocity, and precipitation with simulated dust emissions.

2. Materials and methods

2.1. Model description and setup

Shao et al. (2011) proposed a new size-resolved dust emission scheme (S11):

$$F(d_i,\ d_s) = c_y \eta_f \sigma_p (1 + \sigma_m) g \frac{Q_{ds}}{u_*^2} \tag{1}$$

where $F(d_i,\ d_s)$ is the dust emission rate for particles of size d_i generated by the saltation of particles of size d_s, c_y is a dimensionless coefficient, η_f is the fraction of dust that can be emitted, σ_p is the ratio between the fraction of free dust and that of aggregated dust, σ_m is the bombardment efficiency, g is the acceleration due to gravity, Q_{ds} is the saltation flux of particles of size d_s, and u_* is friction velocity. The dust emission of size d_i is the estimation of a weighted average over the particle size range from d_1 to d_2:

$$F(d_i) = \int_{d_1}^{d_2} F(d_i; d_s)\ p_s(d)\delta d \tag{2}$$

where $p_s(d)$ is the minimally disturbed particle size distribution of the parent soil to constrain the size distribution of the airborne sand and dust particles. The S11 scheme is a simplification of Shao (2004) dust emission scheme (S04). Comparisons show that performances of the full scheme (S04) and the simplified scheme (S11) are equally effective (Shao et al., 2011). Both the Air Force Weather Agency (AFWA) and S11 schemes have been used to simulate dust emissions over East Asia, but the AFWA scheme omits almost the entire Gobi Desert and produces low dust emissions. However, the S11 scheme has better performance in reproducing surface particulate matter 10 μm or less in diameter (PM_{10}) concentrations than the AFWA emission scheme, especially at those stations near the Gobi Desert (Su and Fung, 2015).

The S11 scheme has been implemented in the Weather Research and Forecasting model with chemistry (WRF-Chem) since 2013 (Su and Fung, 2015). Five dust size bins (0–2 μm, 2–3.6 μm, 3.6–6 μm, 6–12 μm, and 12–20 μm) are considered in the S11 scheme from WRF-Chem version 3.7.1. In this work, S11 is adopted to simulate dust emissions simultaneously with the meteorological fields in China and Mongolia (Fig. S1) from 1980 to 2015. The Goddard Chemistry Aerosol Radiation and Transport (GOCART) chemical model and S11 dust emission scheme are used in this study. Dust is simulated as a tracer using the tracer option available in WRF-Chem without considering anthropogenic emissions and chemistry. The tracer option only simulates emissions, transport, and removal processes of dust particles.

The simulation domain is defined on the Lambert projection. The model domain is centered at 100° E, 41° N, and covers nearly the entire East Asia region. All simulations are conducted using a horizontal grid resolution of 36-km with a vertical grid resolution of 28 levels. The model domain has 140 and 100 grid points in the west-east and south-north directions, respectively. Geographical data including elevation dataset, soil properties, albedo, land use, etc. are interpolated primarily from USGS (United States Geological Survey data) at 10-min resolution.

To parameterize the atmospheric processes, six model setting options (Table 1) are conducted for the period of 1 January 2010 to 31 December 2010. The best performance of wind speed among the six model settings is adopted to simulate dust emissions over East Asia for the period of 1 December 1979 to 31 December 2015. The first month of outputs are considered as model spin up and excluded from the analysis to minimize the effect of initial conditions on the results. The instantaneous model output was stored every hour and has been used for the analysis.

The initial and lateral boundary conditions for the meteorological fields were provided from the National Centers for Environmental Prediction (NCEP)-National Center for Atmospheric Research (NCAR) Reanalysis Project (NNRP) (Kalnay et al., 1996). These data are available every 6 h with a spatial resolution of 2.5° and 17 pressure levels. To limit the errors in the WRF-simulated meteorology, four-dimensional data assimilation (FDDA) has been applied. In the FDDA, temperature is nudged at all the vertical levels

Table 1
WRF-Chem configuration options of meteorological evaluation experiments.

Model options	SIM1	SIM2	SIM3	SIM4	SIM5	SIM6
Longwave radiation	RRTM LW	RRTM LW	RRTM LW	RRTM LW	RRTM LW	RRTM LW
Shortwave radiation	RRTM SW	RRTM SW	RRTM SW	RRTM SW	RRTM SW	RRTM SW
Surface layer	Revised MM5 MO	Revised MM5 MO	Revised MM5 MO	MO	Revised MM5 MO	MO
Microphysics	Morrison 2-mom	Morrison 2-mom	Morrison 2-mom	Morrison 2-mom	Morrison 2-mom	Morrison 2-mom
Land Surface	Noah LSM	Noah LSM	Noah LSM	Noah LSM	Noah LSM	Noah LSM
Cumulus Parameterization	Grell-Freitas ensemble	Multi-scale Kain-Fritsch	Multi-scale Kain-Fritsch	Multi-scale Kain-Fritsch	Multi-scale Kain-Fritsch	Multi-scale Kain-Fritsch
Wind correction	Jimenez	Jimenez	UW	Off	UW	Off
Urban surface	Off	Off	Off	MLBEP	MLBEP	MLBEP
Planetary Boundary Layer	Yonsei University	Yonsei University	Yonsei University	Mellor-Yamada- Janjic	Yonsei University	Mellor-Yamada- Janjic

RRTM LW, the Rapid Radiative Transfer Model longwave radiation model; RRTM SW, the Rapid Radiative Transfer Model shortwave radiation model; Revised MM5 MO, Revised fifth-generation Pennsylvania State University-National Center for Atmospheric Research Mesoscale Model (MM5) Monin-Obukhov; MO, Monin-Obukhov; Morrison 2-mom, Morrison Two-Monent Stratiform Cloud Microphysics scheme; Noah LSM, Noah Land Surface Model; UW, Bretherton and Park scheme; MLBEP, Multi-layer, Building Environment Parameterization scheme.

with a nudging coefficient of 0.0003. The horizontal winds are nudged at all vertical levels, except within the planetary boundary layer (PBL), with the nudging coefficient of 0.0003. The nudging coefficients for temperature and winds have been chosen following previous studies (Liu et al., 2012; Mar et al., 2016). The time step for the simulations has been set at 120 s.

2.2. Observational datasets

We begin by evaluating the modelled meteorological fields against observations which are driving the simulations of dust emissions due to WRF-Chem couples the meteorology simulations online with the chemistry. In this study, the WRF-Chem-simulated meteorological fields are evaluated against the 3-hourly in situ measurements of 2 m temperature (T2), 10 m wind velocity and direction (WSP10 and WDR10, respectively), and precipitation (PCP) at 469 meteorological stations (Fig. S1) from the National Oceanic and Atmospheric Administration (NOAA) - National Climatic Data Center Surface (NCDC). These meteorological variables were selected for the evaluation as these are expected to have significant influences on dust emissions, which is the main focus of this study. Moreover, the simulated meteorological datasets are also used to analyze the impacts of the changing climate on dust emissions.

Since the scarcity of observational surface dust emissions, the simulated PM (particulate matter) concentrations, including PM_{10}, particulate matter 2.5 μm or less in diameter ($PM_{2.5}$), and coarse particulate matter with diameter between 2.5 and 10 μm ($PM_{10\text{-}2.5}$), are evaluated against the in situ measurements of PM concentrations from the Ministry of Environmental Protection of the People's Republic of China. PM_{10} concentrations during the period of 2000–2013 are derived from Air Pollution Indexes (API) because only the PM_{10} concentrations are observed and delivered in API in most cities of China before 2014. The API is defined as a semi-quantitative measure for uniformly reporting air quality, and it is based on a set of atmospheric constituents that have implications for human health (Qu et al., 2010). For the days when PM_{10} was reported as primary, daily PM_{10} concentrations can be derived from the APIs using the following equation:

$$C = \frac{(I - I_{low})\left(C_{high} - C_{low}\right)}{I_{high} - I_{low}} + C_{low} \tag{3}$$

where C is the concentration of PM_{10}, I is the API reported. I_{low} and I_{high} represent API grading limits that are lower and larger than I, respectively. C_{high} and C_{low} denote the PM10 concentrations corresponding to I_{high} and I_{low}, respectively. Further details of API and the conversion between API and PM_{10} concentrations can be found in Qu et al. (2010). Observed PM_{10}, $PM_{2.5}$, and $PM_{10\text{-}2.5}$ concentrations are used to evaluate the model performance of dust simulations during the period of 2014–2015 is due to the PM_{10} and $PM_{2.5}$ concentrations are observed and released after 2014 in most cities of China.

To minimize the impact of background concentrations and anthropogenic sources, this study assumes that dust event outbreaks occur when simulated surface PM_{10} and $PM_{2.5}$ concentrations are greater than 20 μg m^{-3} and 10 μg m^{-3}, respectively. Only the PM_{10} and $PM_{2.5}$ concentrations of dust events are included in the model evaluations. Moreover, $PM_{10\text{-}2.5}$ concentrations are also used to evaluate the model performance due to the dust emission is the main contributor to coarse particles.

2.3. Evaluation methodology

Stations are adopted to evaluate the performance of dust simulations over dust source regions. Spatial distributions of the surface meteorological and chemical sites are shown in Fig. S1. Evaluations of meteorological variables, PM_{10}, $PM_{2.5}$, and $PM_{10\text{-}2.5}$ concentrations are conducted using the protocol introduced by Wang et al. (2009). The statistical measures used here include the mean bias (MB), the normalized mean bias (NMB), the normalized mean error (NME), the root mean square error (RMSE), and correlation coefficient (R) (Zhang et al., 2006). Further details of their calculation method can be referenced in Liu et al., 2016. Six WRF-Chem experimental simulations with different configurations (Table 1) are evaluated against the observational data at 469 meteorological stations from NCDC over China and Mongolia for the period of 1 Janurary 2010 to 31 December 2010, and then the dust concentrations simulated by WRF-Chem are initialized on 1 December 1979 and run through 31 December 2015 using the configuration of the best performance for wind velocities among the six experimental simulations. The performance of meteorological simulations (T2, WSP10, WDR10, and PCP) are also evaluated by using the 3-hourly in situ observations at 469 sites (Fig. S1) in China and Mongolia during the study period of 1980–2015.

3. Results and discussion

3.1. Evaluation of meteorology

Wind velocity is the primary driving factor for dust emissions (Kim and Choi, 2015). Performance statistics for meteorological variables in 2010 (Table S1) indicate that wind velocities from all the six sensitivity simulations are overpredicted. Such overpredictions have also been reported in other studies (Liu et al., 2016). Model setup options of SIM3 (Table 1) give the lowest MB (0.4 m s^{-1}), NMB (12.4%), NME (56.5%), and RMSE (2.2 m s^{-1}) and the highest R (0.5) (Table S1) among the six sensitivity simulations. This study uses the configurations of SIM3 in WRF-Chem to simulate dust emissions over the past four decades due to its better performance of wind velocities than other sensitivity simulations (Table S1). Table 2 shows a summary of domain-wide statistics evaluating the seasonal model simulation against observations in meteorological variables of T2, WSP10, WDR and PCP during the period of 1980–2015.

The spatial distribution of seasonal average T2 in the model and observations is shown in Fig. S2, along with the spatial variation in mean bias and temporal (3-hourly) correlation. Overall, the spatial variability in observed T2 is found to be well reproduced by WRF-Chem during all the seasons. The absolute values of mean biases in T2 were generally found to be lower than 1.5 °C (Fig. S2). T2 is often underpredicted in most parts of the research domain, but it is overpredicted over southern parts of China during spring and northern parts of China and Mongolia during summer. The *R* values are generally found to be more than 0.9 in all the seasons and show no significant geographical variation except parts of northern China in winter, indicating that the model is able to reproduce the hourly variations in near-surface temperature. The mean bias in T2 varies −1.1 to −0.2 °C depending on the seasons (Table 2).

The spatial variations of wind speeds, including the seasonality, with strongest winds in winter, have been reproduced by WRF-Chem (Fig. S3). However, the model tends to overpredict and underpredict wind speeds with absolute large biases (1 m s^{-1} or more) during the winter and autumn in southern and northern parts of the domain, respectively. The temporal correlation of wind speed is generally above 0.6 in most parts of the research domain. However, the temporal correlation is lower (<0.4) in some regions of the domain, including southern parts of the domain during the autumn and winter, some areas of northern parts of the domain during the spring and summer. Similar behaviour for simulated wind speed are also reported by some previous studies (Zhang et al., 2013; Liu et al., 2016; Mar et al., 2016). These studies attributed the uncertainties in wind speeds primarily to the poor representation of the surface drag caused by the unresolved topographical feature with a coarse grid resolution of 36-km.

Statistics for wind direction at the research domain is presented in Table 2, with the spatial distribution shown in Fig. S4. Wind direction over northern parts of East Asia is predominantly from west and north during the winter, spring, and autumn, but it is predominantly from east and south in southern China during these seasons. However, the wind direction is from east and south over most parts of the domain in summer. The mean bias of wind direction in most areas of the domain is between −30 and 30° depending on the seasons. In southern China, the wind direction has largest biases and the lowest temporal correlations that may be caused by the complex topography in these areas. Although the temporal correlation of the WSD10 is lower (<0.7) during all the seasons, simulated wind velocity, including wind speeds and wind direction, can be reasonably used to drive the dust emission model because the wind speed on the land surface is the primary driving force for the dust emission.

The spatial distribution of seasonal mean precipitation in the model and measurements is shown in Fig. S5, along with the spatial variabilities in mean bias and temporal correlation. The precipitation is lower in northern parts of this domain. The lowest and strongest precipitation during the winter and summer have been reproduced by the model, respectively. In most regions, however, the model tends to overestimate the precipitation with biases (0–2 mm day^{-1}) except some areas of southern parts of China depending on the seasons. The temporal correlation of precipitation is generally above 0.3 over most parts of the domain, but Mongolia region has the lowest correlation may be caused by the lower precipitation and uncertainties of the observational precipitation in this region. Overall, the WRF-Chem model adopted in this study is capable of reproducing the spatial and temporal variations in the East Asia meteorological conditions reasonably well over the past four decades.

3.2. Evaluation of dust concentrations

To evaluate the performance of dust concentrations simulated by WRF-Chem, the API (2000–2013) at 8 sites and observational PM (PM_{10} and $PM_{2.5}$) concentrations (2014–2015) at 18 sites are adopted due to the scarcity of the dust emission rate observations. These sites are in dust source regions and the anthropogenic emissions are lower than other sites in eastern China (Fig. S1) (Zhang and Fang, 2015), which means that the impacts of background concentrations and anthropogenic sources are weaker than the sites in other regions. Both the surface PM_{10} (Fig. 1; Table 3) and $PM_{2.5}$ (but do not show here) concentrations are underpredicted. Averaged MB, NMB, NME, RMSE, and R of PM_{10} and $PM_{2.5}$ concentrations are −56.5 and −29.1 μg m^{-3}, -44.0% and −55.4%, 2.4%

Table 2
Domain-wide seasonal statistical performance of WRF-Chem against 3-hourly meteorological observations from NCDC during the period of 1980–2015.

Variables	Seasons	MeanObs	MeanSim	MB	NMB(%)	NME(%)	RMSE	R
T2 (°C)	DJF	−0.8	−1.9	−1.1	−0.5	2.6	3.5	0.9
	MAM	6.1	5.2	−0.9	−15.1	37.9	3.4	0.9
	JJA	21.9	21.7	−0.2	−0.1	8.9	3.3	0.9
	SON	18.7	17.8	−0.9	−4.6	9.3	3.1	0.9
WSP10 (m s^{-1})	DJF	1.9	3.2	1.3	69.0	76.1	1.7	0.4
	MAM	2.5	3.5	1.0	43.0	51.1	1.5	0.5
	JJA	2.2	3.2	1.0	42.1	49.8	1.3	0.5
	SON	1.9	2.9	1.0	49.4	56.4	1.3	0.5
WDR10 (degree)	DJF	210.5	190.1	−20.4	−12.7	46.9	189.0	0.2
	MAM	206.4	185.2	−21.3	−13.4	47.3	165.2	0.2
	JJA	201.5	167.3	−34.2	−15.6	47.3	194.7	0.2
	SON	211.4	172.7	−38.7	−16.3	48.6	192.7	0.2
PCP (mm day^{-1})	DJF	0.9	0.7	−0.2	−10.6	107.3	6.4	0.5
	MAM	2.8	2.4	−0.4	−17.2	97.8	9.5	0.4
	JJA	3.5	4.3	0.8	12.2	139.7	7.3	0.5
	SON	1.8	2.1	0.3	7.2	123.6	8.5	0.3

DJF-winter, MAM-spring, JJA-summer, SON-autumn.

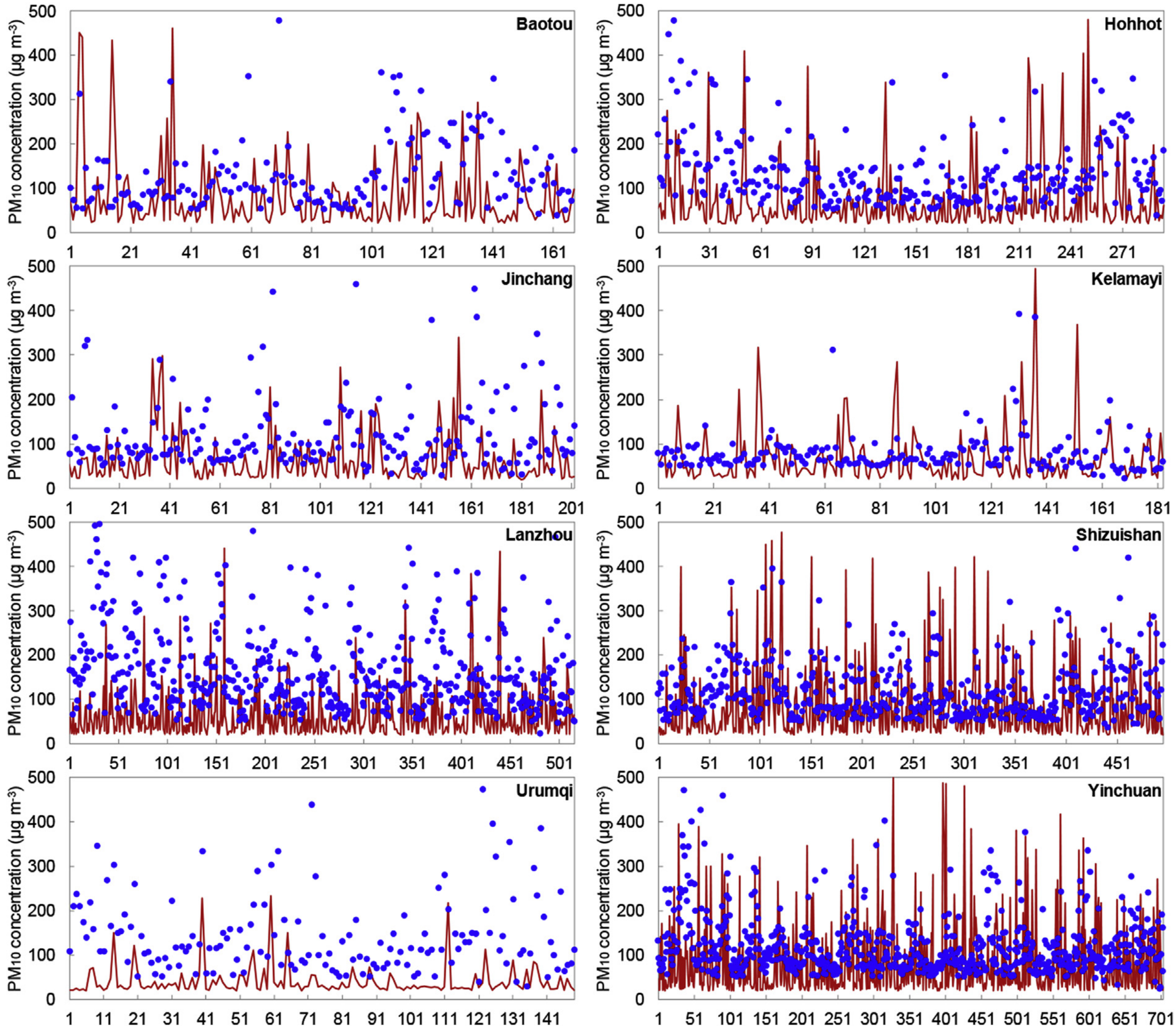

Fig. 1. Series of observed (>20 μg m^{-3}) (blue circles) and simulated (red lines) surface PM_{10} concentrations at eight sites (red stars in Fig. S1.) in China during 2000–2015. *X* axises denote days of simulated PM_{10} concentrations are greater than 20 μg m^{-3} from 2000 to 2015. (For interpretation of the references to colour in this figure legend, the reader is referred to the web version of this article.)

and 63.5%, 115.4 and 56.6 μg m^{-3}, and 0.2 and 0.2, respectively. The best performance of PM_{10} concentrations is at Karamay with MB, NMB, NME, RMSE, and R of −11.7 μg m^{-3}, -14.7%, 58.9%, 70.4 μg m^{-3}, and 0.3, respectively (Table 3). The large discrepancy between simulations and observations of PM_{10} and $PM_{2.5}$ may be attributed in part to the potential errors of meteorological simulations, such as the underpredicted or overpredicted wind velocity and precipitation would contribute to the uncertain of particulate matters. This model cannot well represent the effect of precipitation on vegetation coverage, which would result in uncertainties of dust emissions. Moreover, the simulations without anthropogenic emissions, the default dust boundary conditions, and biases in the dust emission scheme adopted in this study could also result in the uncertain of particulate matter simulations.

Table 3
Model performance statistics of surface PM_{10} concentrations at eight observation sites during 2000–2015.

Observation Sites	MeanObs	MeanSim	MB	NMB(%)	NME(%)	RMSE	R
Baotou	131.3	79.9	−51.4	−39.1	69.1	122.0	0.1
Hohhot	135.3	71.2	−64.1	−47.4	70.1	122.8	0.1
Jinchang	119.4	63.2	−56.2	−47.1	61.6	106.8	0.2
Karamay	79.5	67.8	−11.7	−14.7	58.9	70.4	0.3
Lanzhou	162.3	62.7	−99.6	−61.4	69.2	143.2	0.1
Shizuishan	119.6	83.3	−36.3	−30.3	64.5	101.2	0.2
Urumqi	142.7	41.4	−101.4	−71.0	72.3	129.9	0.3
Yinchuan	119.1	81.3	−37.8	−31.8	67.5	106.5	0.1

Similar to the simulations of PM_{10} and $PM_{2.5}$, all the coarse particulates of $PM_{10-2.5}$ concentrations are underpredicted at the 18 measurement sites (Fig. 2; Table 4). However, the R value of correlations between simulated $PM_{10-2.5}$ concentrations and observed $PM_{10-2.5}$ concentrations are greater than 0.4 (Table 4). The domain-wide of the MB, NMB, NME, RMSE, and R of $PM_{10-2.5}$ are −40.8 μg m^{-3}, -45.1%, 62.0%, 83.5 μg m^{-3}, and 0.5, respectively. The WRF-Chem without the anthropogenic emissions can simulate better $PM_{10-2.5}$ concentrations than concentrations of PM_{10} and $PM_{2.5}$, and it also indicates that the dust emission is the main contributor to the coarse particulate matter. This is consistent with the results reported in several previous studies (Reid et al., 2003; Achilleos et al., 2016). Although the surface PM concentrations are underpredicted to some extent, the S11 in WRF-Chem can simulate well the $PM_{10-2.5}$ concentrations which is mainly caused by the dust emissions and it can well simulate the spatial and

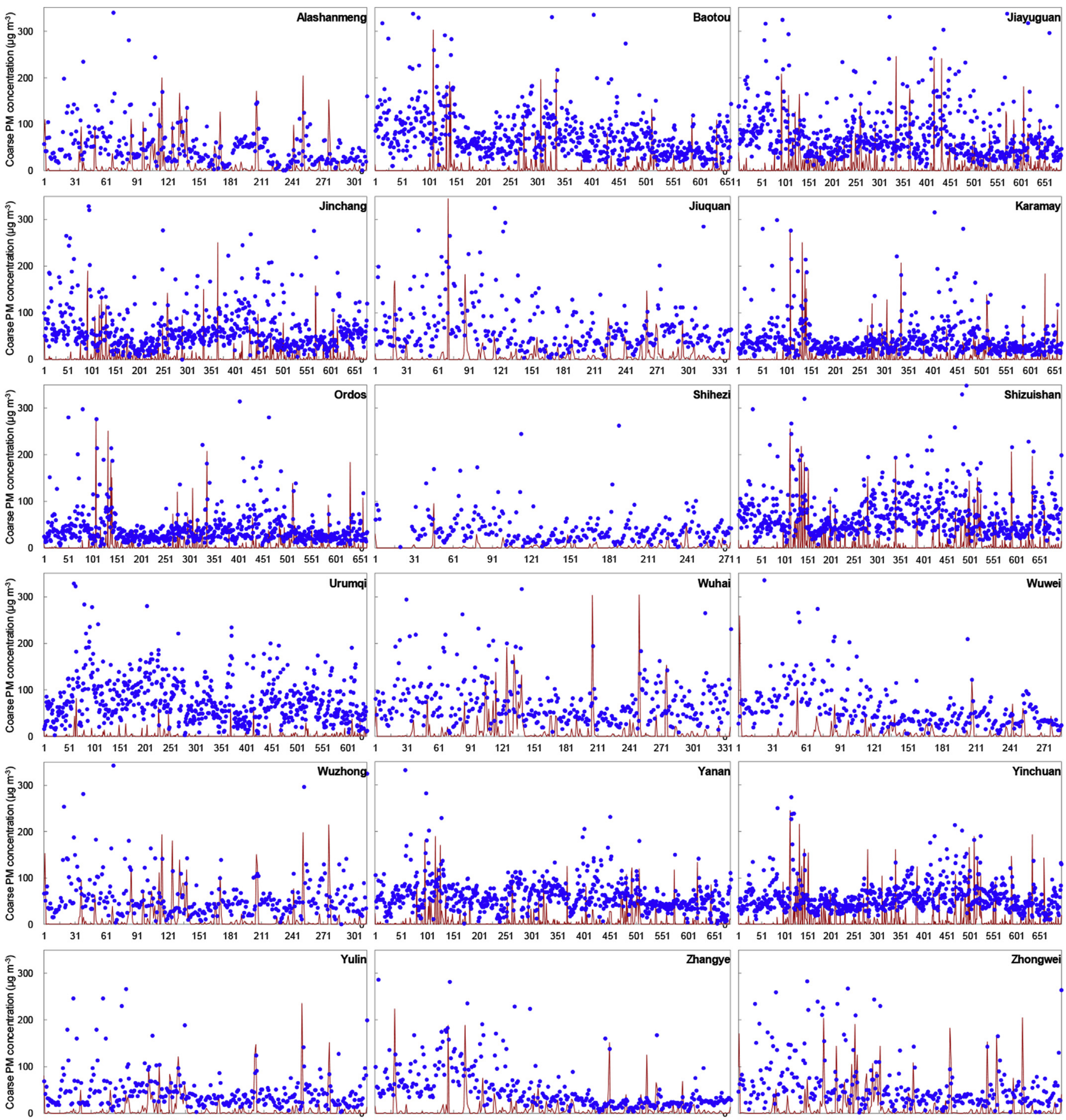

Fig. 2. Series of observed (blue circles) and simulated (red lines) $PM_{10\text{-}2.5}$ concentrations at 18 sites (black triangles in Fig. S1.) in China during 2014–2015. *X* axises denote days of simulated PM_{10} concentrations during 2014–2015. (For interpretation of the references to colour in this figure legend, the reader is referred to the web version of this article.)

temporal variations of dust emissions.

3.3. *Trends in dust emissions and meeteorology*

Fig. 3 illustrates the interannual variations in annual mean dust emissions ($0 < r < 20$ μm), wind velocity, precipitation, and temperature over dust source regions (Fig. 5a) during 1980–2015. At the regional scale, the average annual dust emission is ~67.4 Tg yr^{-1} and the dust emission insignificantly increased with the trend of 0.173 Tg yr^{-1} ($R^2 = 0.03$, $P = 0.32$) (Fig. 3a) in China and Mongolia over the past four decades. The maximum and minimum annual dust emissions are 95.38 Tg in 2001 and 45.94 Tg in 2003 (Fig. 3a). There are three clearly distinct periods of 1980–1991, 1992–1999, and 2000–2013 over the entire study period although the trends are not statistically significant. The annual dust emissions generally decreases by -0.45 Tg yr^{-1} ($P = 0.41$) between 1980 and 1991, but slightly increases from 60.03 Tg in 1991 to 72.98 Tg in 1992 and then declines by -0.56 Tg yr^{-1} ($P = 0.66$) until 1999. However, the

Table 4
Model performance statistics of surface $PM_{10-2.5}$ concentrations at 18 observation sites during 2014–2015.

Observation Sites	MeanObs	MeanSim	MB	NMB(%)	NME(%)	RMSE	R
Alashanmeng	75.9	57.0	−18.9	−24.9	59.2	62.3	0.4
Baotou	68.3	44.0	−24.3	−48.3	65.2	66.0	0.6
Jiayuguan	113.8	48.8	−64.9	−57.1	67.5	120.1	0.5
Jinchang	98.2	52.5	−45.7	−46.5	57.5	101.9	0.6
Jiuquan	116.9	53.6	−63.3	−54.1	66.4	108.9	0.5
Karamay	59.7	40.2	−19.5	−32.6	64.6	62.5	0.4
Ordos	53.7	41.4	−12.4	−22.8	57.7	40.2	0.6
Shihezi	56.5	22.5	−34.0	−60.1	62.8	47.1	0.7
Shizuishan	104.3	52.7	−51.6	−49.5	62.9	99.3	0.4
Urumqi	92.1	27.3	−64.8	−70.3	72.3	86.2	0.6
Wuhai	109.1	54.6	−54.5	−49.9	65.1	92.2	0.7
Wuwei	88.2	37.1	−51.1	−57.9	61.9	93.5	0.6
Wuzhong	84.2	53.5	−30.7	−36.5	56.1	67.1	0.4
Yanan	87.0	50.8	−36.2	−41.6	54.3	57.1	0.4
Yinchuan	77.9	49.9	−28.0	−35.9	57.0	65.2	0.5
Yulin	74.7	49.7	−25.0	−33.3	52.1	51.1	0.6
Zhangye	76.4	41.7	−34.7	−45.3	66.3	73.2	0.5
Zhongwei	98.1	69.6	−28.5	−29.1	63.3	80.2	0.4

annual dust emission steadily increases by 0.51 yr^{-1} ($P = 0.52$) from 1999 to 2013 and then decreases during 2013–2015.

Both wind velocity ($R^2 = 0.13$, $P < 0.05$) (Fig. 3b) and precipitation ($R^2 = 0.11$, $P < 0.05$) (Fig. 3c) increase significantly with trends of 0.0023 m s^{-1} yr^{-1} and 0.97 mm yr^{-1} in dust source regions over the past four decades. Increasing dust emission is parallel with increasing wind velocity (Fig. 3b). Dust emission is positively correlated with wind speed ($R = 0.49$, $P < 0.01$) (Fig. 4a), but it is negatively correlated with precipitation ($R = -0.34$, $P < 0.05$) (Fig. 4b) across the dust source regions. This is consistent with previous studies (Kim and Choi, 2015; Largeron et al., 2015; Webb et al., 2016), suggesting that wind and precipitation can stimulate and inhibit dust emissions, respectively. Our results suggest that at the regional scale, dust emission is more strongly regulated by wind velocity ($R^2 = 0.24$, $P < 0.01$) (Fig. 4a) than by precipitation ($R^2 = 0.12$, $P < 0.05$) (Fig. 4b). The temperature slightly increases by 0.008 °C yr^{-1} during the study period ($R^2 = 0.02$, $P = 0.357$) (Fig. 3d) and the correlation between dust emission and temperature is not significant ($R = 0.13$, $P = 0.46$) (Fig. 4c).

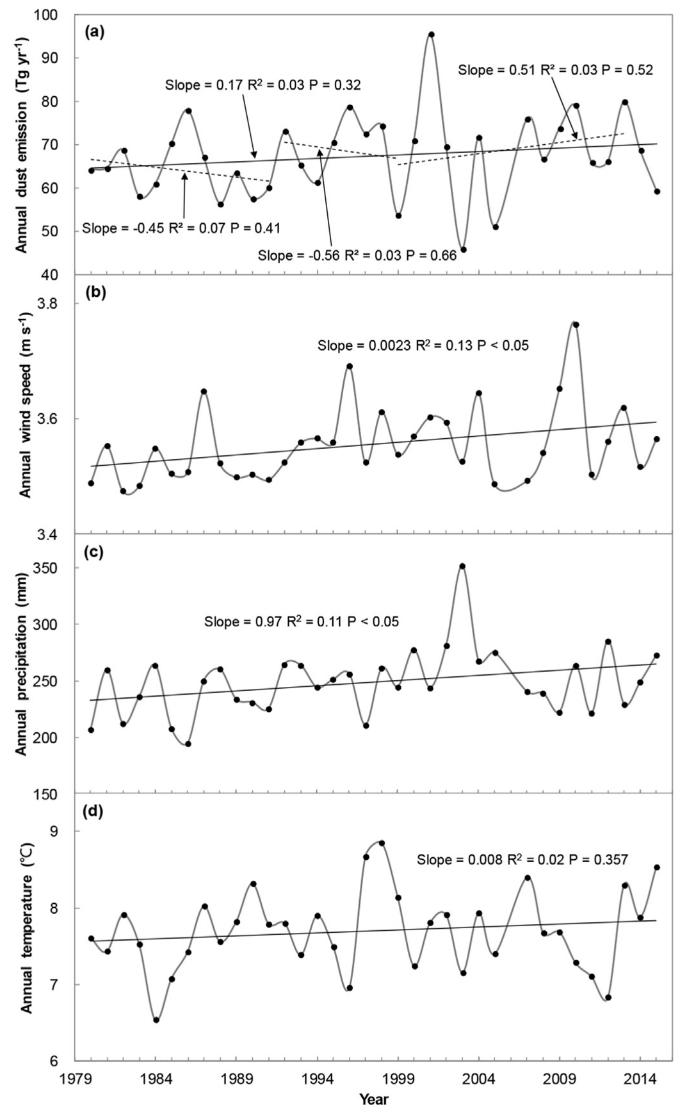

Fig. 3. Inter-annual variations of dust emissions (a), wind speed (b), precipitation (c), and temperature (d) over dust source regions in China and Mongolia during the period of 1980–2015. Solid lines indicate linear fit during the period 1980–2015; dashed lines in (a) indicate linear fit during the period of 1980–1991, 1992–1999, and 2000–2013.

3.4. *Spatial patterns of trends in dust flux*

Dust source regions are mainly located in northwestern China and southern Mongolia, including Taklimakan Desert, Badain Jaran Desert, Tengger Desert, Ulan Buh Desert, Hexi Corridor in Gansu, and Gobi Desert in Xinjiang, Gansu, western Inner Mongolia, and southern Mongolia (Fig. 5a). The vegetation cover and precipitation in these regions are lower than 20% and 400 mm yr^{-1} (Song et al., 2016), respectively. The simulated annual dust flux is more than 20 g m^{-2} yr^{-1} in most severe dust source regions during 1980–2015. The annual dust flux in areas of Badain Jaran Desert, Tengger Desert, and Ulan Buh Desert can be up to >150 g m^{-2} yr^{-1}. Lower dust flux in Taklimakan Desert is due to the lower percentage of the simulated particles with diameter ≤20 μm in the particle size distribution of this region. The largest and lowest seasonal dust fluxes occur in spring and winter, respectively (Figs. S6 and S7).

Dust emissions increase ($P < 0.25$) (Fig. S8) in Taklimakan Desert, southeastern Mongolia, and western Inner Mongolia, but decrease in Gobi areas of eastern Xinjiang, northwestern Gansu, and western Inner Mongolia (Fig. 4b) during 1980–2015. Spatial patterns of trends in seasonal dust fluxes vary greatly in dust source regions over the past four decades (Figs. 5c–f). Dust emissions mainly occur in spring in China and Mongolia (Figs. S6 and S7). Dust flux increase ($P < 0.25$) (Figs. 5c, 5e, and S9a) over most dust source regions both in spring and autumn, but decrease over regions of Hexi Corridor and parts of eastern Xinjiang in spring (Fig. 5c). In summer, however, the dust flux declines in most parts of dust source areas and increases in parts of Xinjiang and Hexi Corridor (Fig. 5d). Although the dust flux is lowest in winter (Figs. S6 and S7), it shows an upward tendency in northwestern Inner Mongolia and southeastern parts of Taklimakan Desert (Figs. 5f and S9d).

3.5. *Spatial patterns of trends in meteorology*

Although increasing trends of annual mean wind velocity, precipitation, and temperature are apparent over dust source areas at the regional scale, we find a high degree of spatial heterogeneity that varies seasonally (Fig. 6). Wind speed tends to increase in most dust source regions in seasons of spring (Fig. 6a), autumn (Fig. 6g), and winter (Fig. 6j), but decreases in southeastern Mongolia and most regions of Inner Mongolia in summer (Fig. 6d). Precipitation tends to elevate in most dust regions (Figs. 6b and h) in spring and autumn, especially in areas of southern Inner Mongolia and Hexi

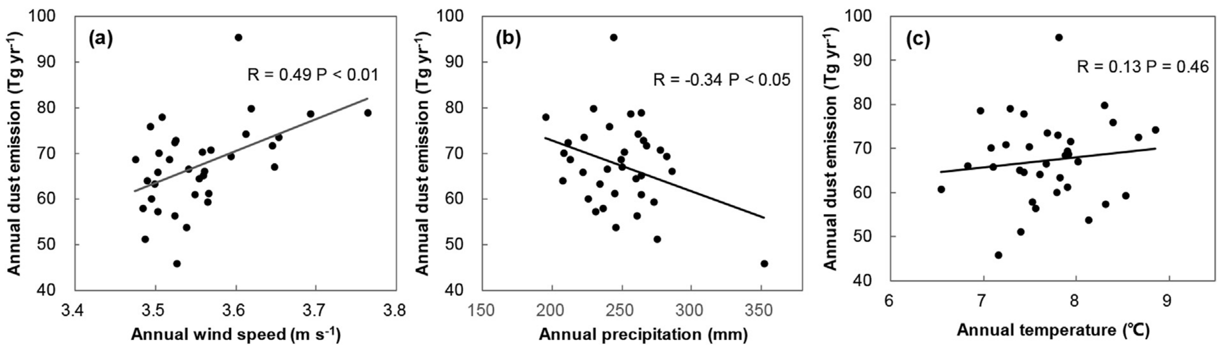

Fig. 4. Correlations between (a) annual dust emissions and wind speed, (b) annual dust emissions and precipitation, and (c) annual dust emissions and temperature over dust source regions in China and Mongolia from 1980 to 2015.

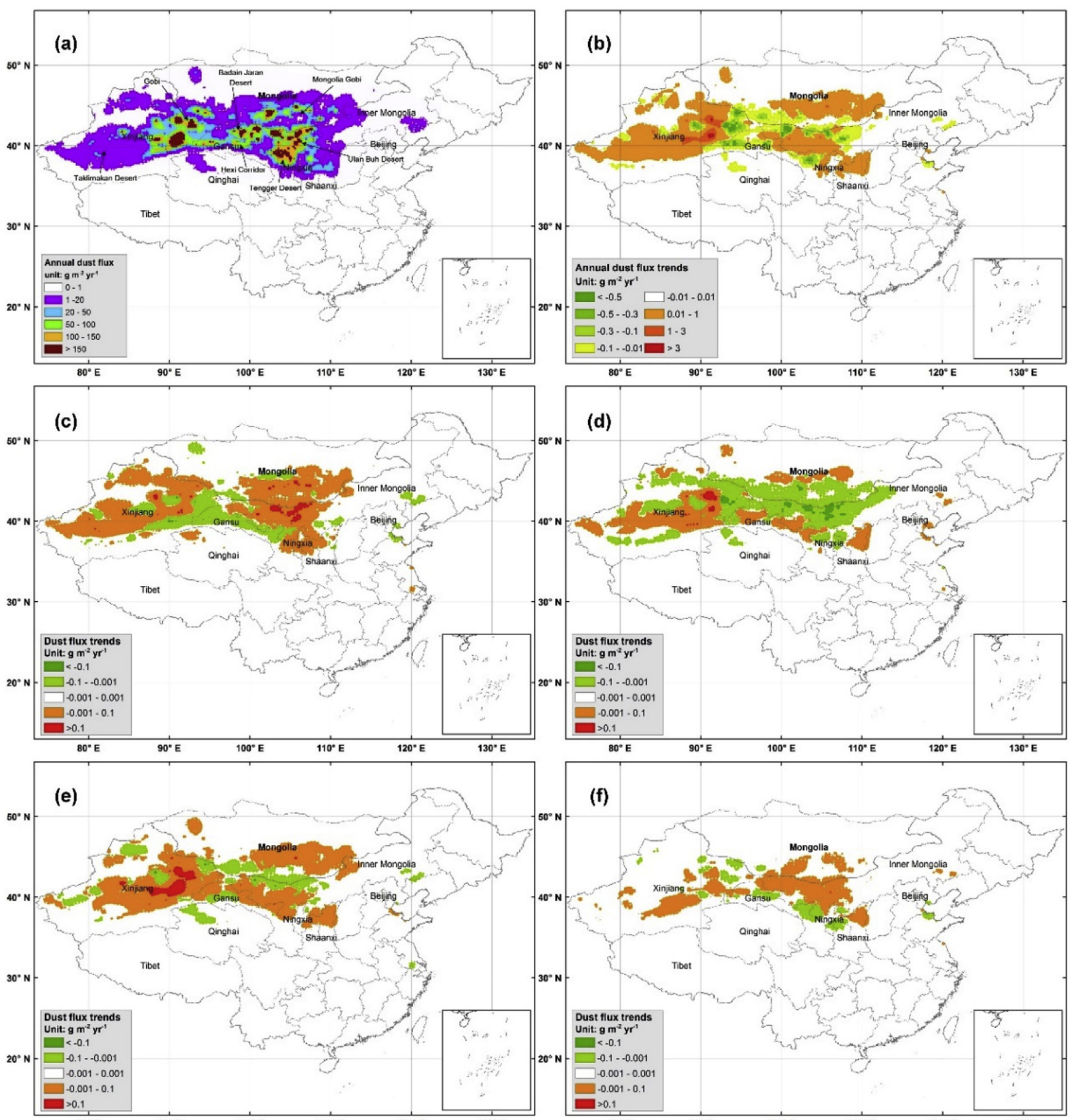

Fig. 5. Spatial patterns of (a) annual mean dust fluxes, (b) annual dust flux trends, trends of the dust flux in (c) spring, (d) summer, (e) autumn, and (f) winter over China and Mongolia from 1980 to 2015.

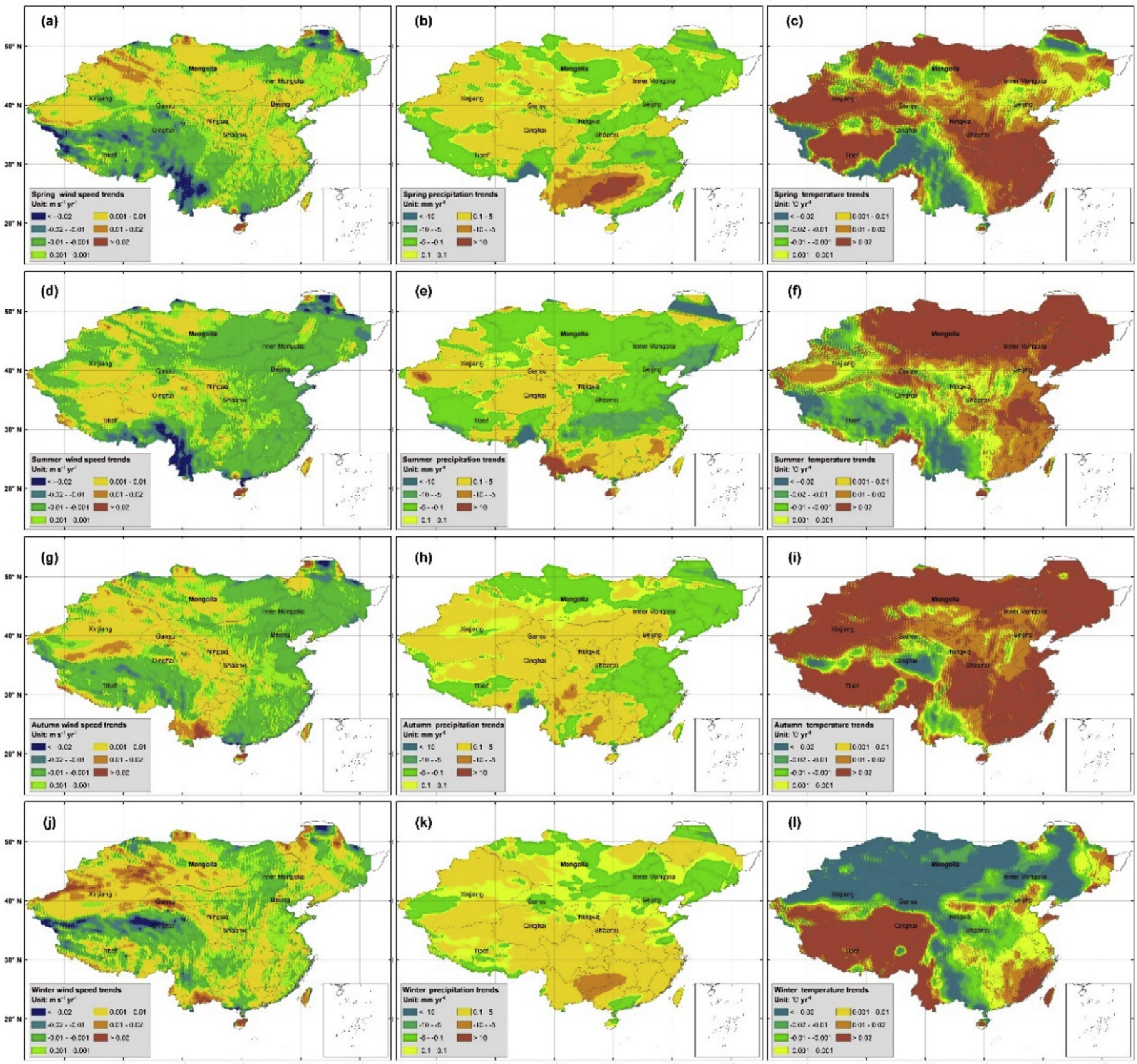

Fig. 6. Spatial patterns of trends of wind speed in (a) spring, (d) summer, (g) autumn, and (j) winter, precipitation in (b) spring, (e) summer, (h) autumn, and (k) winter, and temperature in (c) spring, (f) summer, (i) autumn, and (l) winter in China and Mongolia during 1980–2015.

Corridor in autumn, but declines significantly in parts of Mongolia (Figs. 6b, 6h, and S11). In summer, however, precipitation declines significantly in most regions of Mongolia (Figs. 6e and S11b). The temperature increases in most dust regions during seasons of spring (Fig. 6c), summer (Fig. 6f), and autumn (Fig. 6i), but decreases in parts of Mongolia in spring and northwestern Xinjiang in summer (Figs. 6c, 6f, 6i, and S12). In winter, however, the temperature decreases in most dust source regions (Figs. 6l and S12d) from 1980 to 2015.

3.6. Spatial patterns of correlations between dust emission and meteorology

To analyze effects of regional climates on seasonal dust emissions, correlations between dust flux and climate (wind speed, precipitation, and temperature) were showed for seasons of spring, summer, autumn, and winter (Fig. 7). Strong significantly ($P < 0.05$) (Fig. S13) positive correlations are identified between seasonal dust flux and wind velocity (Figs. 7a, d, g, and j) for all four seasons, but dust emission in summer is more strongly and positively correlated with wind speed (Figs. 7d and S13) than in other three seasons. Moreover, we also identify that the correlation between dust emission and wind speed is more strongly in eastern dust source regions than in western dust source areas for all four seasons. This indicates that wind velocity could be the primary driving force for the dust emissions across dust source areas of China and Mongolia. This result is consistent with the finding of Kim and Choi (2015) that surface wind speed is the main factor determining the

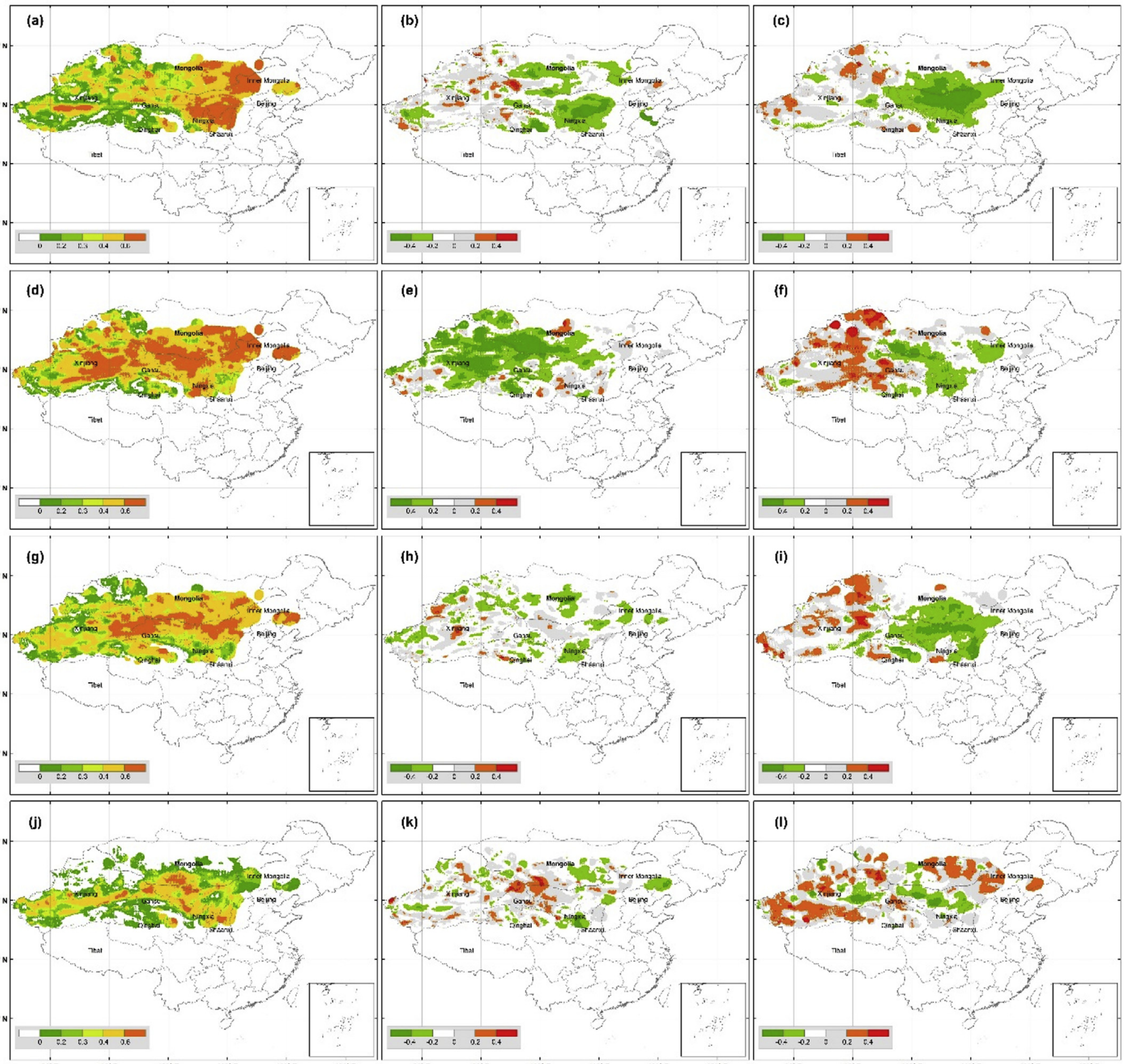

Fig. 7. Spatial patterns of correlations between dust emission and wind speed in (a) spring, (d) summer, (g) autumn, and (j) winter, between dust emission and precipitation in (b) spring, (e) summer, (h) autumn, and (k) winter, and between dust emission and temperature in (c) spring, (f) summer, (i) autumn, and (l) winter in China and Mongolia.

mobilization of sand and dust in dust source regions.

Spatial patterns of seasonal correlations between dust flux and precipitation varies greatly during the period of 1980–2015 (Figs. 7b, e, h, and k). In spring, dust emission is negatively correlated with precipitation ($P < 0.05$) (Fig. S14a) in western Inner Mongolia, Ningxia, and parts of Mongolia (Fig. 7b). Precipitation has negative impacts on dust emissions in regions of most Xinjiang province except Taklimakan Desert, southwestern Mongolia, and parts of Hexi Corridor (Figs. 7e and S14b). In autumn and winter, however, dust emission is not significantly correlated with precipitation over most dust source regions (Figs. 7h, 7k, S14c, and S14d). Most dust source regions are arid areas with mean annual precipitation less than 200 mm. In western China, precipitations mainly occur in summertime and precipitation increase has been observed over the past several decades (Zhai et al., 2005). Precipitation has no or weak impacts on dust emissions across most dust source regions in spring, autumn, and winter is due to precipitation cannot significantly shift the soil moisture and general surface characteristics that can directly prohibit dust emissions (Yang et al., 2007; Munkhtsetseg et al., 2016). In summer, however, precipitation can inhibit dust emissions in Gobi areas of China is due to surface sandy soils in Gobi regions mixed with bare rocks and soil moisture could be easily changed by summer precipitation. Moreover, vegetation in Gobi areas is highly sensitive to precipitation and small changes in precipitation can significantly alter the vegetation cover (Xu et al., 2006). The dust outbreaks exponentially decrease by increasing the minimum threshold wind friction velocity due to increasing soil moisture (Kim and Choi, 2015; Bergametti et al., 2016) and vegetation cover (Tegen et al., 2004), which could be the main mechanism of the negative impact of precipitation on dust emissions in Gobi Desert areas of China in summer.

Numerous studies have demonstrated that wind speed and precipitation can directly impact dust emissions in dust source regions (Tegen et al., 2004; Kim and Choi, 2015), but the mechanism of impacts of temperature on dust emission is not clear although several studies have conducted to explore the relationship between dust emission and temperature (Yang et al., 2007; Lee and Sohn, 2011). Here we analyzed the relationship between dust flux and temperature and identified that the temperature has negative impacts on dust emissions in southern Mongolia, western Inner Mongolia, and Hexi Corridor in spring and autumn, but the dust flux in parts of Xinjiang is positively correlated with temperature (Figs. 7c, 7i, S15a, and S15c). Similar to autumn, dust flux is negatively correlated with temperature in western Inner Mongolia and southeastern Mongolia and is positively correlated with temperature in summer (Fig. 7f). Although the mechanism of impacts of the temperature on dust emission is not definitely known, significant ($P < 0.05$) correlations between the dust emission and temperature has been discovered, such as western Inner Mongolia in spring and autumn. Several studies reported that the temperature change can indirect/direct shift the patterns of wind speed, precipitation, soil moisture (Shukla and Misra, 1977; Aldrian and Dwi Susanto, 2003; Trenberth and Shea, 2005), and thus dust emissions. This may be one mechanism of the relationship between dust emission and temperature.

4. Conclusions

This study simulates and evaluates the performance of WRF-Chem in meteorological variables and particulate matter concentrations without anthropogenic emissions, and then simulates spatial and temporal variations of dust emissions in China and Mongolia from 1980 to 2015. Based on simulations of the dust emission and meteorology, correlations between dust emissions and wind velocity, precipitation, and temperature are examined over the past four decades. The annual dust flux increases in Desert areas of China and southern Mongolia, but decreases in most parts of Gobi Desert of China during the period of 1980–2015. These results demonstrate the model's capability in simulating dust emissions and the impact of the changing climate on changes in dust emissions over East Asia. Although uncertainties in dust emission simulations remain due to the use of fixed land use dataset, not well represent the effect on precipitation and vegetation coverage in WRF-Chem, uncounted interactions between dust emissions and anthropogenic emissions, and the uncertain of wind velocity and precipitation, several significant impacts of meteorological factors on dust emissions in dust source regions are identified over the past four decades.

Acknowledgements

HS and SZ are financially supported by the National Natural Science Foundation of China (41401107), the China Sponsorship Council (201408410206), the Postdoctoral Research Program of Henan Province (2014028), and the Research Program of Henan University (2015YBZH001). YZ, KW, and CH are supported by the National Science Foundation EaSM program (AGS-1049200) at NCSU. Thanks are due to Patrick Campbell from NCSU for helpful discussions on data analysis. Thanks are also due to the Super Computing Center of Henan University, Kaifeng, China.

Appendix A. Supplementary data

Supplementary data related to this article can be found at http://dx.doi.org/10.1016/j.atmosenv.2017.08.051.

References

Achilleos, S., Wolfson, J.M., Ferguson, S.T., Kang, C.M., Hadjimitsis, D.G., Hadjicharalambous, M., Achilleos, C., Christodoulou, A., Nisanzti, A., Papoutsa, C., Themistocleous, K., 2016. Spatial variability of fine and coarse particle composition and sources in Cyprus. Atmos. Res. 169, 255–270. http://dx.doi.org/10.1016/j.atmosres.2015.10.005.

Aldrian, E., Dwi Susanto, R., 2003. Identification of three dominant rainfall regions within Indonesia and their relationship to sea surface temperature. Int. J. Climatol. 23, 1435–1452. http://dx.doi.org/10.1002/joc.950.

Allen, R.J., Landuyt, W., Rumbold, S.T., 2016. An increase in aerosol burden and radiative effects in a warmer world. Nat. Clim. Change 6, 269–274. http://dx.doi.org/10.1038/nclimate2827.

Bergametti, G., Rajot, J.L., Pierre, C., Bouet, C., Marticorena, B., 2016. How long does precipitation inhibit wind erosion in the Sahel? Geophys. Res. Lett. 43, 6643–6649. http://dx.doi.org/10.1002/2016GL069324.

Cowie, S.M., Knippertz, P., Marsham, J.H., 2013. Are vegetation-related roughness changes the cause of the recent decrease in dust emission from the Sahel? Geophys. Res. Lett. 40, 1868–1872. http://dx.doi.org/10.1002/grl.50273.

Evan, A.T., Flamant, C., Fiedler, S., Doherty, O., 2014. An analysis of aeolian dust in climate models. Geophys. Res. Lett. 41, 5996–6001. http://dx.doi.org/10.1002/2014GL060545.

Evan, A.T., Flamant, C., Gaetani, M., Guichard, F., 2016. The past, present and future of African dust. Nature 531, 493–495. http://dx.doi.org/10.1038/nature17149.

Fiedler, S., Kaplan, M.L., Knippertz, P., 2015. The importance of Harmattan surges for the emission of North African dust aerosol. Geophys. Res. Lett. 42, 9495–9504. http://dx.doi.org/10.1002/2015GL065925.

Haywood, J., Allan, R., Culverwell, I., Slingo, T., Milton, S., Edwards, J., Clerbaux, N., 2005. Can desert dust explain the outgoing longwave radiation anomaly over the Sahara during July 2003? J. Geophys. Res. 110, D05105. http://dx.doi.org/10.1029/2004JD005232.

Hoffman, A.L., Forest, C.E., Li, W., 2014. Estimating the sensitivity of regional dust sources to sea surface temperature patterns. J. Geophys. Res. Atmos. 119, 10,160–10,174. http://dx.doi.org/10.1002/2014JD021682.

Ishizuka, M., Mikami, M., Yamada, Y., Zeng, F., Gao, W., 2005. An observational study of soil moisture effects on wind erosion at a gobi site in the Taklimakan Desert. J. Geophys. Res. 110, D18S03. http://dx.doi.org/10.1029/2004JD004709.

Kalnay, E., Kanamitsu, M., Kistler, R., Collins, W., Deaven, D., Gandin, L., Iredell, M., Saha, S., White, G., Woollen, J., Zhu, Y., Leetmaa, A., Reynolds, R., 1996. The NCEP/NCAR 40-year reanalysis project. Bull. Amer. Meteor. Soc. 77, 437–471. http://dx.doi.org/10.1175/1520-0477(1996)077<0437:TNYRP>2.0.CO;2.

Kim, H., Choi, M., 2015. Impact of soil moisture on dust outbreaks in East Asia: using satellite and assimilation data. Geophys. Res. Lett. 42, 2789–2796. http://dx.doi.org/10.1002/2015GL063325.

Kok, J., 2011. A scaling theory for the size distribution of emitted dust aerosols suggests climate models underestimate the size of the global dust cycle. Proc. Natl. Acad. Sci. U. S. A. 108 (3), 1016–1021. http://dx.doi.org/10.1073/pnas.1014798108.

Kurosaki, Y., Mikami, M., 2005. Regional difference in the characteristic of dust event in East Asia: relationship among dust outbreak, surface wind, and land surface condition. J. Meteorol. Soc. Jpn. 83A, 1–18. http://dx.doi.org/10.2151/jmsj.83A.1.

Lambert, F., Delmonte, B., Petit, J.R., Bigler, M., Kaufmann, P.R., Hutterli, M.A., Stocker, T.F., Ruth, U., Steffensen, J.P., Maggi, V., 2008. Dust-climate couplings over the past 800,000 years from the EPICA Dome C ice core. Nature 452, 616–619. http://dx.doi.org/10.1038/nature06763.

Lambert, F., Kug, J.S., Park, R.J., Mahowald, N., Winckler, G., Abe-Ouchi, A., O'ishi, R., Takemura, T., Lee, J.H., 2013. The role of mineral-dust aerosols in polar temperature amplification. Nat. Clim. Change 3, 487–491. http://dx.doi.org/10.1038/nclimate1785.

Largeron, Y., Guichard, F., Bouniol, D., Couvreux, F., Kergoat, L., Marticorena, B., 2015. Can we use surface wind fields from meteorological reanalyses for sahelian dust emission simulations? Geophys. Res. Lett. 42, 2490–2499. http://dx.doi.org/10.1002/2014GL062938.

Lee, E.H., Sohn, B.J., 2011. Recent increasing trend in dust frequency over Mongolia and Inner Mongolia regions and its association with climate and surface condition change. Atmos. Environ. 45, 4611–4616. http://dx.doi.org/10.1016/j.atmosenv.2011.05.065.

Lee, J.J., Kim, C.H., 2012. Roles of surface wind, NDVI and snow cover in the recent changes in Asian dust storm occurrence frequency. Atmos. Environ. 59, 366–375. http://dx.doi.org/10.1016/j.atmosenv.2012.05.022.

Lelieveld, J., Evans, J.S., Fnais, M., Giannadaki, D., Pozzer, A., 2015. The contribution of outdoor air pollution sources to premature mortality on a global scale. Nature 525, 367–371. http://dx.doi.org/10.1038/nature15371.

Lim, J.Y., Chun, Y.S., 2006. The characteristics of Asian dust events in Northeast Asia during the springtime from 1993 to 2004, global planet. Change 52, 231–247. http://dx.doi.org/10.1016/j.gloplacha.2006.02.010.

Liu, X.Y., Zhang, Y., Zhang, Q., He, K.B., 2016. Application of online-coupled WRF/

Chem-MADRID in East Asia: model evaluation and climatic effects of anthropogenic aerosols. Atmos. Environ. 124, 321–336. http://dx.doi.org/10.1016/j.atmosenv.2015.03.052.

Liu, P., Tsimpidi, A.P., Hu, Y., Stone, B., Russell, A.G., Nenes, A., 2012. Differences between downscaling with spectral and grid nudging using WRF. Atmos. Chem. Phys. 12, 3601–3610. http://dx.doi.org/10.5194/acp-12-3601-2012.

Liu, X., Yin, Z.Y., Zhang, X., Yang, X., 2004. Analyses of the spring dust storm frequency of northern China in relation to antecedent and concurrent wind, precipitation, vegetation, and soil moisture conditions. J. Geophys. Res. Atmos. 109, D16210. http://dx.doi.org/10.1029/2004JD004615.

Mahowald, N.M., Ballantine, J.A., Feddema, J., Ramankutty, N., 2007. Global trends in visibility: implications for dust sources. Atmos. Chem. Phys. 7, 3309–3339. http://dx.doi.org/10.5194/acp-7-3309-2007.

Mar, K.A., Ojha, N., Pozzer, A., Butler, T.M., 2016. Ozone air quality simulations with WRF-Chem (v3. 5.1) over Europe: model evaluation and chemical mechanism comparison. Geosci. Model Dev. 9, 3699–3728. http://dx.doi.org/10.5194/gmd-9-3699-2016.

Munkhtsetseg, E., Shinoda, M., Gillies, J.A., Kimura, R., King, J., Nikolich, G., 2016. Relationships between soil moisture and dust emissions in a bare sandy soil of Mongolia. Particuology 28, 131–137. http://dx.doi.org/10.1016/j.partic.2016.03.001.

Nagashima, K., Suzuki, Y., Irino, T., Nakagawa, T., Tada, R., Hara, Y., Yamada, K., Kurosaki, Y., 2016. Asian dust transport during the last century recorded in Lake Suigetsu sediments. Geophys. Res. Lett. 43, 2835–2842. http://dx.doi.org/10.1002/2015GL067589.

Natsagdorj, L., Jugder, D., Chung, Y.S., 2003. Analysis of dust storms observed in Mongolia during 1937–1999. Atmos. Environ. 37 (9), 1401–1411. http://dx.doi.org/10.1016/S1352-2310(02)01023-3.

Pointing, S.B., Belnap, J., 2014. Disturbance to desert soil ecosystems contributes to dust-mediated impacts at regional scales. Biodivers. Conserv. 23, 1659–1667. http://dx.doi.org/10.1007/s10531-014-0690-x.

Qian, W., Quan, L., Shi, S., 2002. Variations of the dust storm in China and its climatic control. J. Clim. 15, 1216–1229. http://dx.doi.org/10.1175/1520-0442(2002)015<1216:VOTDSI>2.0.CO;2.

Qu, W.J., Arimoto, R., Zhang, X.Y., Zhao, C.H., Wang, Y.Q., Sheng, L.F., Fu, G., 2010. Spatial distribution and interannual variation of surface PM_{10} concentrations over eighty-six Chinese cities. Atmos. Chem. Phys. 10, 5641–5662. http://dx.doi.org/10.5194/acp-10-5641-2010.

Ravi, S., D'Odorico, P., Over, T.M., Zobeck, T.M., 2004. On the effect of air humidity on soil susceptibility to wind erosion: the case of air-dry soils. Geophys. Res. Lett. 31, L09501. http://dx.doi.org/10.1029/2004GL019485.

Reid, J.S., Jonsson, H.H., Maring, H.B., Smirnov, A., Savoie, D.L., Cliff, S.S., Reid, E.A., Livingston, J.M., Meier, M.M., Dubovik, O., Tsay, S.C., 2003. Comparison of size and morphological measurements of coarse mode dust particles from Africa. J. Geophys. Res. 108, D8593. http://dx.doi.org/10.1029/2002JD002485.

Shao, Y.P., 2004. Simplification of a dust emission scheme and comparison with data. J. Geophys. Res. 109, D10202. http://dx.doi.org/10.1029/2003JD004372.

Shao, Y.P., Ishizuka, M., Mikami, M., Leys, J.F., 2011. Parameterization of size-resolved dust emission and validation with measurements. J. Geophys. Res. 116, D08203. http://dx.doi.org/10.1029/2010JD014527.

Shukla, J., Misra, B.M., 1977. Relationships between sea surface temperature and wind speed over the central Arabian Sea, and monsoon rainfall over India. Mon. Weather Rev. 105, 998–1002. http://dx.doi.org/10.1175/1520-0493(1977)105<0998:RBSSTA>2.0.CO;2.

Song, H.Q., Zhang, K.S., Piao, S.L., Wan, S.Q., 2016. Spatial and temporal variations of spring dust emissions in northern China over the last 30 years. Atmos. Environ. 126, 117–127. http://dx.doi.org/10.1016/j.atmosenv.2015.11.052.

Su, L., Fung, J.C.H., 2015. Sensitivities of WRF-Chem to dust emission schemes and land surface properties in simulating dust cycles during springtime over East Asia. J. Geophys. Res. Atmos. 120, 11,215–11,230. http://dx.doi.org/10.1002/2015JD023446.

Sun, J., Zhang, M., Liu, T., 2001. Spatial and temporal characteristics of dust storms in China and its surrounding regions, 1960–1999: relations to source area and climate. J. Geophys. Res. 106, 10,325–10,333. http://dx.doi.org/10.1029/2000JD900665.

Tegen, I., Werner, M., Harrison, S.P., Kohfeld, K.E., 2004. Relative importance of climate and land use in determining present and future global soil dust emission. Geophys. Res. Lett. 31, L05105. http://dx.doi.org/10.1029/2003GL019216.

Trenberth, K.E., Shea, D.J., 2005. Relationships between precipitation and surface temperature. Geophys. Res. Lett. 32, L14703. http://dx.doi.org/10.1029/2005GL022760.

Wang, K., Zhang, Y., Jang, C., Phillips, S., Wang, B., 2009. Modeling intercontinental air pollution transport over the trans-Pacific region in 2001 using the Community Multiscale Air Quality modeling system. J. Geophys. Res. Atmos. 114, D04307. http://dx.doi.org/10.1029/2008JD010807.

Wang, R., Balkanski, Y., Boucher, O., Ciais, P., Peñuelas, J., Tao, S., 2015. Significant contribution of combustion-related emissions to the atmospheric phosphorus budget. Nat. Geosci. 8, 48–54. http://dx.doi.org/10.1038/ngeo2324.

Webb, N.P., Galloza, M.S., Zobeck, T.M., Herrick, J.E., 2016. Threshold wind velocity dynamics as a driver of aeolian sediment mass flux. Aeolian Res. 20, 45–58. http://dx.doi.org/10.1016/j.aeolia.2015.11.006.

Xu, X., Levy, J.K., Zhaohui, L., Hong, C., 2006. An investigation of sand-dust storm events and land surface characteristics in China using NOAA NDVI data, Global Planet. Change 52, 182–196. http://dx.doi.org/10.1016/j.gloplacha.2006.02.009.

Yang, B., Bräuning, A., Zhang, Z., Dong, Z., Esper, J., 2007. Dust storm frequency and its relation to climate changes in Northern China during the past 1000 years. Atmos. Environ. 41, 9288–9299. http://dx.doi.org/10.1016/j.atmosenv.2007.09.025.

Zender, C.S., Kwon, E.Y., 2005. Regional contrasts in dust emission responses to climate. J. Geophys. Res. Atmos. 110, D13201. http://dx.doi.org/10.1029/2004JD005501.

Zhai, P., Zhang, X., Wan, H., Pan, X., 2005. Trends in total precipitation and frequency of daily precipitation extremes over China. J. Clim. 18, 1096–1108. http://dx.doi.org/10.1175/JCLI-3318.1.

Zhang, Y., Sartelet, K., Wu, S.Y., Seigneur, C., 2013. Application of WRF/Chem-MADRID and WRF/Polyphemus in Europe–Part 1: model description, evaluation of meteorological predictions, and aerosol–meteorology interactions. Atmos. Chem. Phys. 13, 6807–6843. http://dx.doi.org/10.5194/acp-13-6807-2013.

Zhang, Y.L., Fang, C., 2015. Fine particulate matter ($PM_{2.5}$) in China at a city level. Sci. Rep. 5, 14884,. http://dx.doi.org/10.1038/srep14884.

Zhang, Y., Liu, P., Pun, B., Seigneur, C., 2006. A comprehensive performance evaluation of MM5-CMAQ for the Summer 1999 Southern oxidants study episode-part I: evaluation protocols, databases, and meteorological predictions. Atmos. Environ. 40, 4825–4838. http://dx.doi.org/10.1016/j.atmosenv.2005.12.043.